



Hydrothermal Synthesis, Crystal Structure and Properties of 1D Zigzag Chain Zinc(II) Coordination Polymer Constructed from Nicotinic Acid and 1,4-Bis(imidazol-1-ylmethyl)benzene

(This article was produced from 6th National Congress of Inorganic Chemistry and was sent to the JOTCSA editorial board for publication)

Güneş Günay Sezer^{1*}  and İlknur Erucar² 

¹Bartın University, Vocational School of Health Services, 74100, Bartın, Turkey

²Ozyegin University, Department of Natural and Mathematical Sciences, Faculty of Engineering, 34794, Istanbul, Turkey

Abstract: A zinc–nicotinate complex, $\{[\text{Zn}(\text{na})_2(\mu\text{-pbix})]\cdot\text{H}_2\text{O}\}_n$ (**1**), was obtained from the reaction of zinc(II) acetate with nicotinic acid (Hna) and 1,4-bis(imidazol-1-ylmethyl)benzene (pbix) in water at 120 °C under hydrothermal conditions and characterized by elemental analysis, IR spectroscopy, single crystal and powder X-ray diffraction. The thermal stability and luminescent property for **1** were also reported. The asymmetric unit of **1** consists of one zinc(II) center, one pbix ligand, two na anions and one non-coordinated water molecule, giving a formula of $\{[\text{Zn}(\text{na})_2(\mu\text{-pbix})]\cdot\text{H}_2\text{O}\}_n$. The Zn(II) ion is coordinated by two nitrogen atoms from two different 1,4-bis(imidazol-1-ylmethyl)benzene ligands and two oxygen atoms from two different nicotinate (na) anions, thus showing a distorted tetrahedral geometry. The adjacent Zn(II) ions are linked into an infinite 1D zigzag chain by 1,4-bis(imidazol-1-ylmethyl)benzene ligands. Grand canonical Monte Carlo (GCMC) simulations were also performed to compute single-component H₂ adsorption isotherms at a pressure range of 0.01–100 bar and at 298 K and 77 K. The maximum H₂ uptake in **1** was found as 68 cm³/g STP at 100 bar and 77 K. This study will be useful to accelerate the hydrothermal synthesis of new coordination polymers for gas storage applications.

Keywords: Coordination polymer, nicotinic acid, N-donor ligand, zinc(II) complex, molecular simulations.

Submitted: June 27, 2017. **Accepted:** September 08, 2017.

Cite this: Günay Sezer G, Erucar I. Hydrothermal Synthesis, Crystal Structure and Properties of 1D Zigzag Chain Zinc(II) Coordination Polymer Constructed from Nicotinic Acid and 1,4-Bis(imidazol-1-ylmethyl)benzene. JOTCSA. 2017;4(sp. is. 1):23–38.

DOI: 10.18596/jotcsa.323787.

***Corresponding author. E-mail:** ggunay@bartin.edu.tr, Tel: +90 3785050083, Fax: +90 378 505 00 82

INTRODUCTION

Coordination polymers (CPs), a class of novel functional hybrid materials, have been received significant attention due to their structural richness and various potential applications in the field of coordination chemistry and material science (1). CPs are formed by the coordination of metal ions with organic linkers (2) and they have been recently used in many different applications such as gas storage (3), separation (4, 5), catalysis (6), chemical sensor (7, 8), and drug delivery (9). The assembly of CPs is significantly influenced by several factors, such as the type of organic linkers and metal ions, and reaction conditions (10). Among these factors, careful choice and design of organic linkers with a specific geometry, configuration, coordination ability, length and steric effects play an important role in the construction of desired CPs (11).

In general, the most common organic building blocks are N-heterocyclic or aromatic polycarboxyl ligands due to their strong coordination abilities and variable coordination modes with extensive hydrogen bonding interactions. Nicotinic acid (Hna), as a good asymmetric bridging ligand with pyridyl-nitrogen and carboxyl-oxygen donor atoms, has been widely used to construct CPs based on the following considerations: (i) It has been proven to be good building blocks for the construction of various multidimensional structures. (ii) It has potential coordination sites involving nitrogen of the pyridine ring and carboxylate oxygen atoms and can coordinate with metal ion via one or two oxygen atoms of carboxylate or the pyridine or both (12-16). In the literature, there are only a few studies that report CPs with a single asymmetric bridging ligand, **Hna**. For example, Vargová *et al.* reported the 3D supramolecular structure, giving a formula of $[\text{Zn}(\text{na})_2(\text{H}_2\text{O})_4]$ (17). Di *et al.* reported synthesis, characterization, and thermodynamic properties of the chelate compound $[\text{Zn}(\text{na})_2 \cdot \text{H}_2\text{O}]_{(s)}$ (18). Similar structures with $M = \text{Mn}, \text{Fe}, \text{Co}, \text{Ni},$ and Cu have also been reported by Caires *et al.* (19). These pioneering studies reveal that different synthetic approaches are required to synthesize CPs.

Recently, mixed-ligand strategy has been widely used to prepare new CPs with diverse structures, promising properties such as well-defined structures, pore sizes, and pore shapes, and large surface areas for different applications (20-22). The combination of Hna and N-containing auxiliary bridging ligands (such as 5-methyltetrazole, 5-methyl-1H-tetrazole, 5-phenyltetrazole, 5-(4-((1H-1,2,4-triazol-1-yl)methyl)phenyl)-1H-tetrazole, 5-amino-tetrazolate, *etc.*) is of great potential to construct higher-dimensional supramolecular networks and novel topology (14, 23-26). For example, Liu *et al.* synthesized two Zn compounds using 5-methyltetrazole, 5-phenyltetrazole, and **Hna** under hydrothermal conditions (14). They reported that due to the synergistic effects

between symmetric and asymmetric ligands, the materials have multifunctional properties such as ferroelectric behaviors and fluorescent properties. In another study, An *et al.* used **Hna**, **Hisona** and 5-methyl-1H-tetrazole to synthesize two different CPs (23). They examined the luminescent properties of these CPs in the solid-state at room temperature and found out that these two CPs emit blue luminescence. Similarly, Gao *et al.* used **Hna**, **Hisona** and 3-amino-1H-1,2,4-triazole to synthesize two different CPs that have two dimensional structures. They also reported that these materials have strong luminescent properties in the solid state at room temperature (24). As literature review shows using mixed-ligand strategy is useful to synthesize new CPs with desired properties. Therefore, we selected **pbix** as the co-ligand in this study because it provides a coordination environment with transition metal ions, resulting in a huge number of structurally diverse and functionally intriguing CPs (27-30). To the best of our knowledge, mixed-ligand CPs constructed from **pbix** with **Hna** have not been reported to date.

Due to the reasons mentioned above, we used the flexible N-donor **pbix**, **Hna**, and Zn(II) metal ion to synthesize a new CP, $\{[\text{Zn}(\text{na})_2(\mu\text{-pbix})]\cdot\text{H}_2\text{O}\}_n$ (**1**) in this work. We reported the hydrothermal synthesis and crystal structure of complex **1**. The structure of complex **1** has been determined by elemental analysis, IR spectroscopy, single crystal and powder X-ray diffraction techniques. The luminescent property and thermal behavior of complex **1** have been also investigated. We finally performed molecular simulations to assess the potential of **1** in H₂ storage applications. The storage of H₂, as an energy carrier, is difficult using conventional methods because extremely high pressures (100 atm) and low temperatures (77 K) are required. The US Department of Energy (DOE) has reported set targets for on-board hydrogen storage systems: 9.0 wt% and 81 g/L by 2015 (31). Recent studies showed that porous materials could be promising to capture H₂ molecules. For example, MOF (metal organic framework)-177 has a hydrogen saturation uptake of 11.0 wt% at about 100 atm and 77 K (31). Due to the physisorption within the pores of the materials, gas molecules can be efficiently adsorbed. However, it is challenging to test each porous material by using purely experimental methods. Molecular simulations are highly useful to predict the gas storage performance of porous materials including CPs, zeolites or MOFs prior to experimental studies. Therefore, we performed grand canonical Monte Carlo (GCMC) simulations to compute single-component H₂ adsorption isotherms at a pressure range of 0.01–100 bar and at 298 K and 77 K. We then compared the H₂ storage performance of **1** with the performance of widely studied MOFs.

MATERIALS AND METHODS

All chemicals were commercially available and were used without further purification. The ligand **pbix** was prepared according to the description in the literature (32-34). Elemental analyses (C, H, and N) were performed on a Perkin-Elmer 2400C Elemental Analyzer. IR spectrum was recorded on a Shimadzu IRAffinity-1 FTIR spectrometer in the range of 700–4000 cm^{-1} . Thermal analysis measurement was carried out using a HITACHI-STA 7300 Thermo Gravimetric Analyzer in a static air atmosphere with a heating rate of 10 $^{\circ}\text{C}/\text{min}$ in the temperature range 30–700 $^{\circ}\text{C}$. Powder X-ray diffraction patterns (PXRD) were recorded on a Rigaku Smartlab X-ray diffractometer operating at 40 kV and 30 mA with Cu-K α radiation ($\lambda = 1.5406 \text{ nm}$). The photoluminescent properties were measured on an FS5 Edinburgh Fluorescence Spectrometer.

Diffraction data for **1** was collected on Bruker APEXII CCD area-detector diffractometer equipped with a graphite monochromated Mo-K α radiation source ($\lambda = 0.71073 \text{ \AA}$) at 296K. The structure was solved by direct methods using the programs OLEX2 (35) and SHELXS-97 (36) with anisotropic thermal parameters for all non-hydrogen atoms. All non-hydrogen atoms were refined anisotropically by full-matrix least-squares methods SHELXL-97 (36). Molecular drawings were obtained by using MERCURY software (37). Crystal data and structure refinement parameters for **1** were presented in Table 1. Selected bond lengths and angles were listed in Table 2 and hydrogen bond parameters were given in Table 3. The crystallographic information file was deposited with the Cambridge Crystallographic Data Center (CCDC) (38), with the reference number 1556343.

Synthesis of $\{[\text{Zn}(\text{na})_2(\mu\text{-pbix})]\cdot\text{H}_2\text{O}\}_n$ (1**):** The mixtures of **Hna** (0.4 mmol, 0.05 g), $\text{Zn}(\text{O}_2\text{CMe})_2\cdot 2\text{H}_2\text{O}$ (0.2 mmol, 0.04 g), **pbix** (0.4 mmol, 0.09 g) and H_2O (10 mL) were stirred at 70 $^{\circ}\text{C}$ for 30 min. Then the clear solution was placed in a Pyrex tube and heated at 120 $^{\circ}\text{C}$ for 72 h. After cooling to room temperature, crystals of **1** were obtained. Anal. calcd. for $\text{C}_{26}\text{H}_{24}\text{N}_6\text{O}_5\text{Zn}$: C 55.18, H 4.27, N 14.85. Found: C 55.17, H 4.42, N 15.05. IR (KBr, cm^{-1}): 3515 w, 3104 w, 2992 w, 1616 s, 1590 s, 1385 vs, 1238 m, 1094 w, 1028 w, 953 w, 842 m, 762 m.

Computational Details: We performed grand canonical Monte Carlo (GCMC) simulations to compute single-component H_2 isotherms in **1** at a pressure range of 0.01–100 bar and at 298 K and 77 K. The crystalline water molecules in complex **1** were removed before simulations. Structural properties of **1** such as density, pore volume, pore limiting diameter (PLD), and largest cavity diameter (LCD) were computed using Zeo⁺⁺ software (39) and enlisted in Table 4. For pore volume calculations, probe radius was set to zero.

As shown in Table 4, complex **1** has a low pore volume ($0.269 \text{ cm}^3/\text{g}$) and small pore sizes ($1.26 \times 2.93 \text{ \AA}$).

In molecular simulations, interactions of H_2 molecules with the complex **1** were described by Lennard-Jones (LJ) 12-6 potential. Van der Waals interactions were only considered to examine H_2 uptake in complex **1**. 13 \AA was used a cutoff radius to calculate energetic interactions. We used the Lorentz-Berthelot mixing rules to estimate adsorbent-adsorbate and adsorbate-adsorbate LJ cross interaction parameters. GCMC simulations consisted of 3×10^7 Monte Carlo steps. Half of the steps (1.5×10^7) were used for equilibration and the remaining steps were used for the production step. Particle insertion, deletion and translation movements were applied. Simulations were started from an empty MOF cell. Each simulation at higher pressure was started from the final configuration of the previous run. Periodic boundary conditions were employed in all simulations. $2 \times 2 \times 2$ unit cell simulation box for each GCMC run was used. All molecular simulations were performed using a rigid framework. The number of adsorbed gas molecules was calculated at equilibrium.

H_2 molecules were modelled with Buch potential as single spheres using united atom model (40). The universal force field (UFF) LJ parameters were used for the atoms of complex **1** (41). The interaction potential parameters for gas molecules and the atoms of complex **1** were given in Table 5. Various computational studies revealed that simulations performed using UFF as a generic force field give reasonable agreement with the experimental data for gas adsorption in nanoporous materials (42, 43). Details of molecular simulations were found in the literature (44).

We also computed single-component adsorption isotherms of H_2 in widely studied MOFs, including CuBTC, MOF-5 and ZIF-8 at 298 K up to 100 bar to compare H_2 storage performance of **1** with those of these materials. These materials are widely studied in the literature for gas storage applications due to their highly porous and robust structures. Crystal structures of these MOFs were taken from CCDC. Similar to complex **1**, structural properties of these materials were calculated using Zeo⁺⁺ software (39).

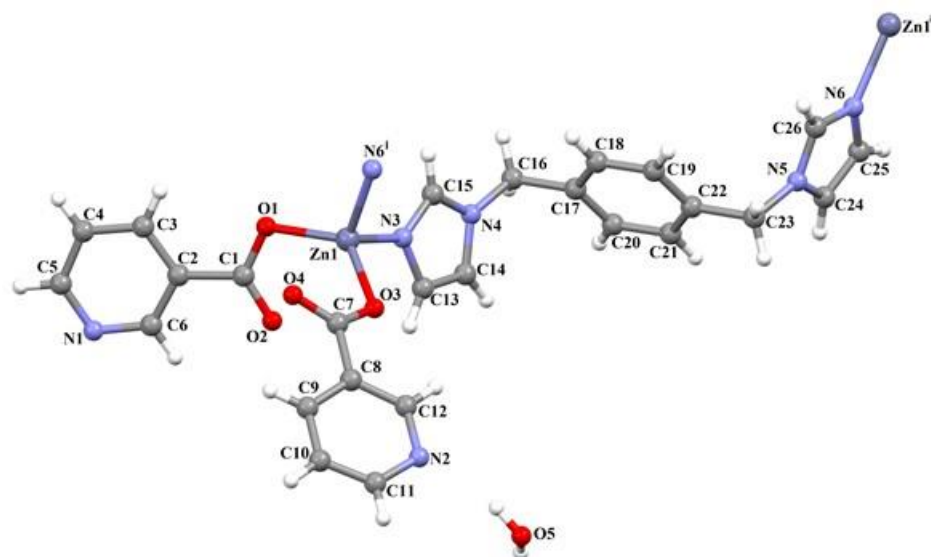
RESULTS AND DISCUSSION

Description of the Crystal Structure:

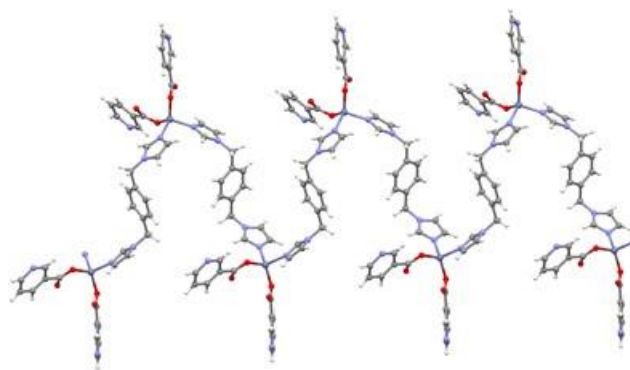
A single crystal X-ray analysis reveals that complex **1** is a CP, possessing 1D zigzag chain structure. Selected bond distances and angles were enlisted in Table 2 and hydrogen bond parameters for **1** were given in Table 3.

As shown in Tables 2 and 3, complex **1** belongs to the monoclinic system with space group $P2_1/n$. The asymmetric unit of **1** consists of one zinc(II) center, one **pbix** ligand, two **na** anions and one non-coordinated water molecule, giving a formula of $\{[\text{Zn}(\text{na})_2(\mu\text{-pbix})]\cdot\text{H}_2\text{O}\}_n$ (Figure 1a). The Zn(II) ion is coordinated by two nitrogen atoms from two different **pbix** ligands and two oxygen atoms from two different **na** anions, thus showing a distorted tetrahedral coordination geometry. In complex **1**, nicotinate coordinated to the Zn(II) ion in a monodentate fashion. Zn(II) ions are linked by the trans-form **pbix** ligands to form a 1D infinite chain (Figure 1b). The Zn...Zn distance separated by **pbix** is 13.655 Å. Adjacent 1D coordination polymers are joined by O5-H5B...N2 and O5-H5A...O1 hydrogen bonds between the uncoordinated water molecules and the carboxyl oxygen/pyridine nitrogen atoms from **na** anions to form a 2D supramolecular network (Figure 1c).

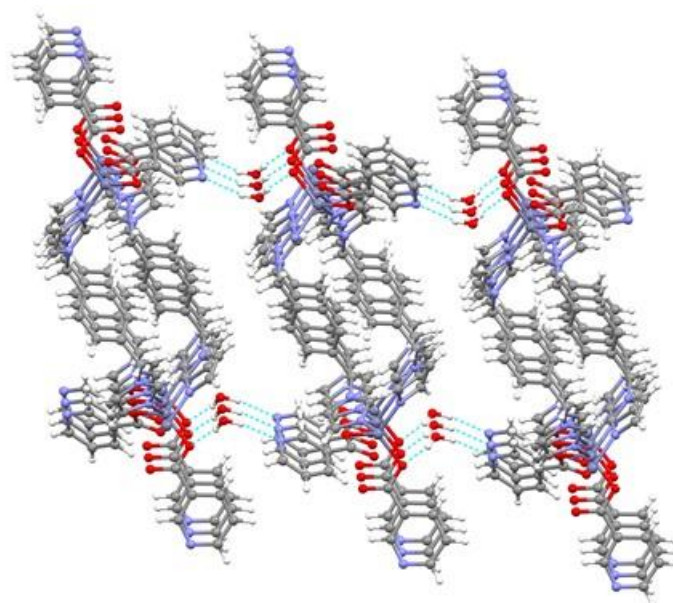
IR spectroscopy of $\{[\text{Zn}(\text{na})_2(\mu\text{-pbix})]\cdot\text{H}_2\text{O}\}_n$ (1**):** The IR spectrum for complex **1** was recorded in the region 4000–700 cm^{-1} by using KBr pellet technique (Figure S1). The IR spectrum of **1** shows broad bands at 3515 cm^{-1} corresponding to the OH stretching vibrations of water. The bands at 1616 and 1385 cm^{-1} are assigned to $\nu_{\text{as}}(\text{COO}^-)$ and $\nu_{\text{s}}(\text{COO}^-)$, respectively. The band difference of $\Delta(\nu_{\text{as}}(\text{COO}^-) - \nu_{\text{s}}(\text{COO}^-))$ exceeds 200 cm^{-1} , which indicates that there is a monodentate coordination mode in **1** (45). No absorption peak between 1576–1579 cm^{-1} for the coordination of the imine nitrogen to the metal is indicated, which confirms that the coordination does not take place through the pyridine ring (46). The result is consistent with the crystal structure of the complex (see Figure 1a). The weak peaks appearing at 3104 and 2992 cm^{-1} are due to aromatic and aliphatic $\nu(\text{C-H})$ stretching vibrations. The strong bands at 1590 cm^{-1} in **1** can be assigned to be the $\nu(\text{C=N})$ absorption in the imidazole ring of **pbix** ligand.



(a)



(b)



(c)

Figure 1: (a) Coordination environment of the Zn(II) ion in **1**, (b) View of the 1D infinite chain in **1** and (c) The 2D supramolecular structure of **1** constructed by hydrogen bonds.

Table 1: Crystal data and structure refinement parameters for structure **1**.

Chemical formula	C ₂₆ H ₂₄ N ₆ O ₅ Zn
FW/ g mol⁻¹	565.88
Temperature (K)	296
Wavelength (Å)	0.71073 Mo Kα
Crystal System	Monoclinic
Space group	<i>P2₁/n</i>
<i>a</i> (Å)	10.6942 (5)
<i>b</i> (Å)	13.8480 (5)
<i>c</i> (Å)	17.4501 (8)
<i>β</i> (°)	91.6760(10)
<i>V</i> (Å³)	2583.14 (19)
<i>Z</i>	4
<i>D_c</i> (Mg m⁻³)	1.455
Absorption coefficient (mm⁻¹)	1.00
<i>θ</i> range (°)	3.4–26.1
Measured reflections	47257
Independent reflections	5274
Observed reflections [<i>I</i> > 2σ(<i>I</i>)]	4181
Final <i>R</i> indices (all data)	<i>R</i> 1 = 0.029 <i>wR</i> 2 = 0.074
<i>R</i>_{int}	0.056
Goodness-of-fit (GOF) on <i>F</i>²	1.02
Δρ_{max} (e Å⁻³)	0.24
Δρ_{min} (e Å⁻³)	-0.29

Table 2: Selected bond lengths (Å) and angles (°) for **1**.

Zn1—O1	1.9727 (12)	Zn1—N3	2.0194 (15)
Zn1—O3	1.9641 (13)	N6—Zn1 ⁱⁱ	2.0309 (15)
Zn1—N6 ⁱ	2.0309 (15)		
O1—Zn1—N6 ⁱ	108.64 (6)	O3—Zn1—N3	103.64 (6)
O1—Zn1—N3	109.27 (6)	N3—Zn1—N6 ⁱ	105.06 (6)
O3—Zn1—O1	124.65 (6)	C26—N6—Zn1 ⁱⁱ	124.92 (13)
O3—Zn1—N6 ⁱ	103.95 (6)	C25—N6—Zn1 ⁱⁱ	129.08 (13)

Symmetry codes: (i) $-x+1/2, y-1/2, -z+1/2$; (ii) $-x+1/2, y+1/2, -z+1/2$.

Table 3: Hydrogen-bond parameters for **1**.

D-H...A	D-H	H...A	D...A	D-H...A
O5—H5A...O1 ⁱⁱⁱ	0.85	2.08	2.918(2)	168
O5—H5B...N2	0.85	2.10	2.929 (3)	165

Symmetry code: (iii) $x-1/2, -y+1/2, z+1/2$.

Powder X-ray Diffraction (PXRD), Photoluminescence and Thermal Properties:

The experimental PXRD patterns of the complex **1** agreed with simulated patterns from its single crystal structure to confirm the phase purity of the complex at room temperature (Figure 2).

Previous studies have shown that CPs based on d¹⁰ metals exhibit photoluminescence properties (23, 24). Solid state photoluminescent spectrum of complex **1** was recorded at room temperature. Figure 3 shows the photoluminescence emission spectra of **1**. This result is consistent with the reported literature (14, 47). These emissions can be attributed to $\pi^* \rightarrow \pi$ transitions. As shown in Figure 3, the intense emission peaks appear at 413 nm ($\lambda_{ex}=340$ nm) for **1**. The emissions for **1** cannot be attributed to metal-to-ligand charge transfer (MLCT) or ligand to metal transfer (LMCT), since the Zn(II) ion is difficult to oxidize or reduce. The emissions of complex **1** can be attributed to the intraligand emissions ($\pi^* \rightarrow \pi$ and/or $\pi^* \rightarrow n$ transition) because similar emissions were also observed for the ligands themselves.

Thermal analysis measurement was carried out to determine the thermal stability of complex **1** in the temperature range of 30-700 °C at in a dry air atmosphere. Figure 4 shows TG analysis of complex **1** at a heating rate of 10 °C/min in air. For **1**, the first weight loss was observed in the range of 30–60 °C corresponded to the removal of free water molecules (found 3.07%, calcd 3.18%). After 240 °C, the anhydrous complex started to decompose and the final decomposed product was ZnO (found 18.00% and calcd 14.31%).

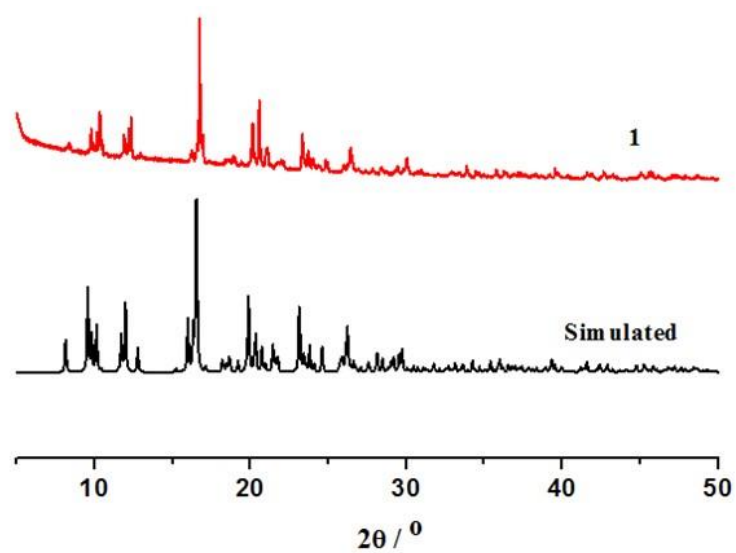


Figure 2: PXRD patterns of complex **1**.

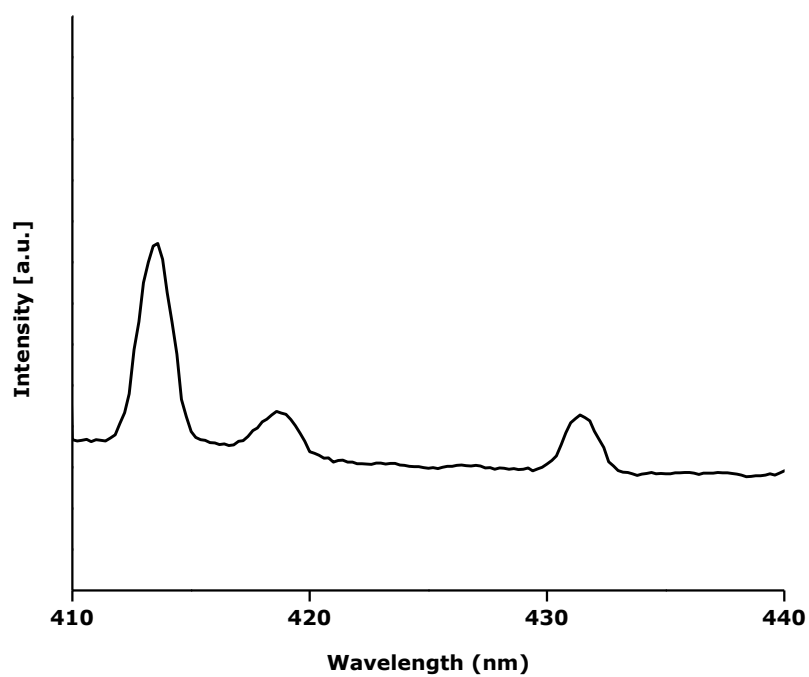


Figure 3: Photoluminescence emission spectrum of complex **1**.

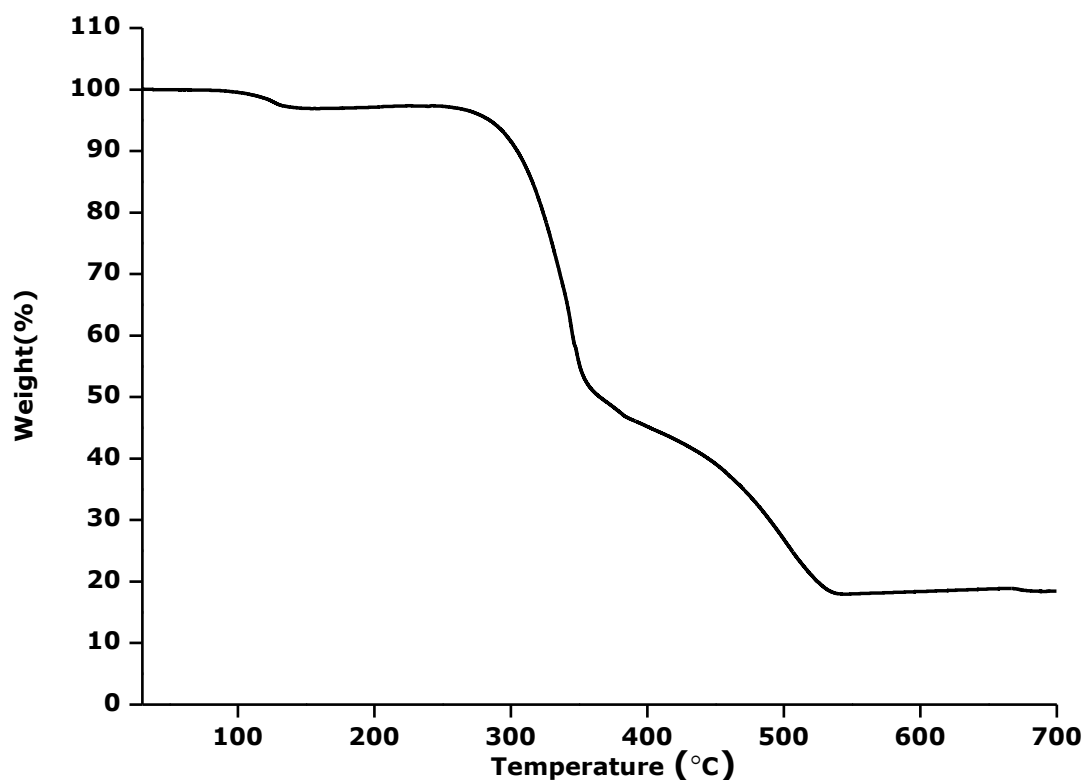


Figure 4: TG curve of **1**.

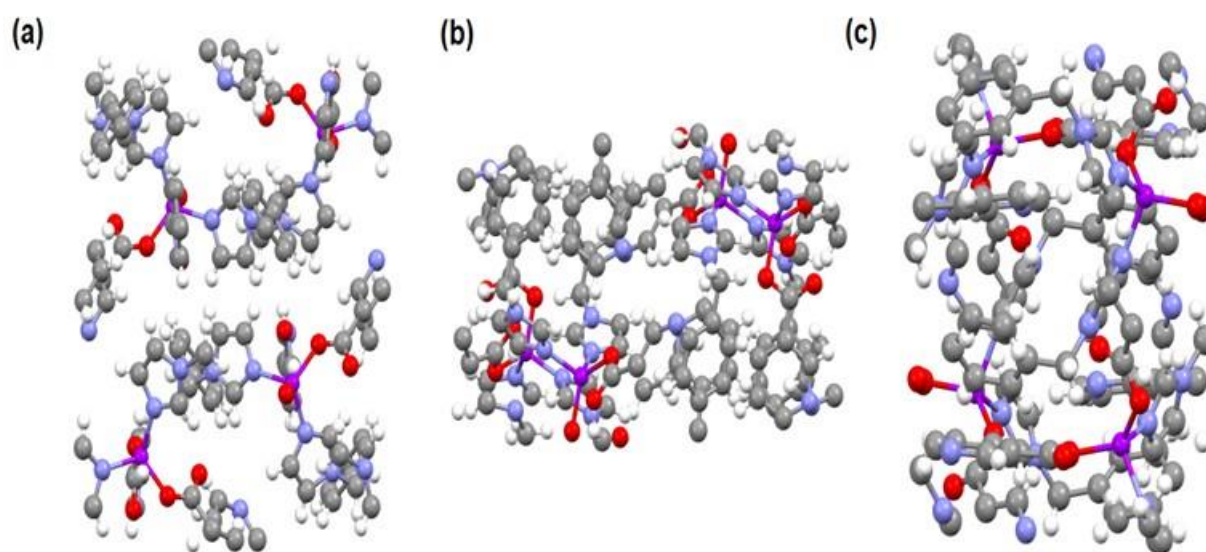
Molecular Simulation Results

We initially computed geometric properties of complex **1** and results were tabulated in Table 4. As shown in Table 4, complex **1** has a low pore volume ($0.269 \text{ cm}^3/\text{g}$) and small pore sizes ($1.26 \times 2.93 \text{ \AA}$). The unit cell representations of complex **1** were given in Figure 5. We then performed GCMC simulations to assess H_2 adsorption performance of complex **1**. We computed single-component H_2 adsorption isotherms of **1** at 77 K and at 298 K and results were shown in Figure 6, which showed that the number of adsorbed H_2 molecules is very low ($1.12 \text{ cm}^3/\text{g STP}$) ((Standard Temperature and Pressure) at 100 bar) at 298 K. However, the number of adsorbed molecules increases with increasing pressure at 77 K and the adsorption isotherm of H_2 is close to saturation. The maximum H_2 uptake capacity of complex **1** is $67.89 \text{ cm}^3/\text{g STP}$) at 100 bar.

We also considered widely studied adsorbents, including CuBTC, MOF-5 and ZIF8, in this work to assess the potential of complex **1** in H_2 storage applications. We computed single-component H_2 adsorption isotherms in these three materials at 298 K up to 100 bar and results were tabulated in Table 6. As shown in Table 6, MOF-5 has the highest H_2 uptake ($145.44 \text{ cm}^3/\text{g STP}$) at 100 bar among these materials. The high H_2 uptake of MOF-5 can be explained by its large surface area ($3655.78 \text{ m}^2/\text{g}$) and high pore volume ($1.36 \text{ cm}^3/\text{g}$). As shown in Table 6, complex **1** has a lower H_2 uptake than these three adsorbent materials. The low H_2 uptake of **1** can be attributed to its low pore volume ($0.269 \text{ cm}^3/\text{g}$). However, the maximum H_2 uptake ($67.89 \text{ cm}^3/\text{g STP}$) of **1** at 77 K can reach the H_2 uptake of ZIF-8 ($71.9 \text{ cm}^3/\text{g STP}$) at 298 K. Therefore, complex **1** can be used as an adsorbent to capture H_2 at 77 K.

Table 4: Structural properties of Complex **1**.

CP	Metals	Pore volume (cm ³ /g)	PLD (Å)	LCD (Å)
Complex 1	Zn	0.269	1.26	2.93

**Figure 5.** Unit cell structure of **1** in x, y, and z directions (from left to right). Red: oxygen, blue: nitrogen, purple: zinc, grey: carbon, white: hydrogen.**Table 5:** Force field parameters for complex **1**, and H₂.

Species	Atom	σ (Å)	ϵ/k_B (K)
	C	3.43	52.87
	H	2.57	22.16
	N	3.26	34.75
	O	3.12	30.21
	Zn	2.46	62.44
H₂	H ₂	2.96	34.20

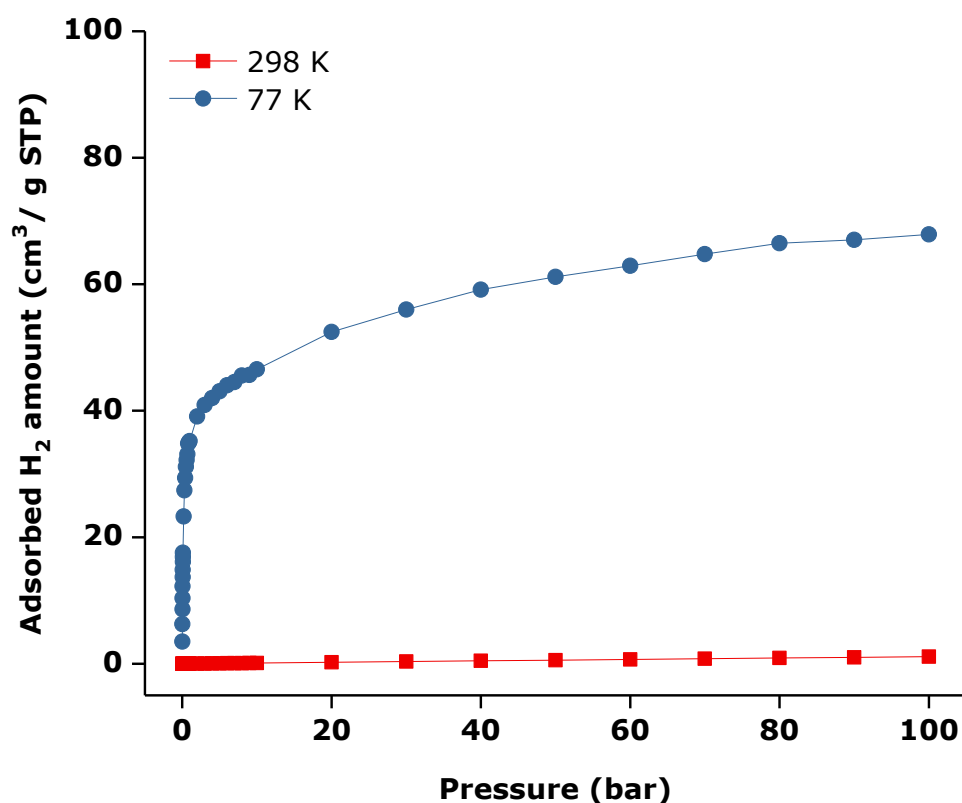


Figure 6: Adsorption isotherms of H₂ in **1** at 298 K and 77 K.

Table 6: Comparison of H₂ uptake (cm³/g STP) in four materials at 298 K.

Adsorbent	0.1 bar	1 bar	10 bar	100 bar
Complex 1	0.001	0.01	0.11	1.12
Cu-BTC	0.14	1.37	13.27	103.47
MOF-5	0.18	1.77	17.40	145.44
ZIF-8	0.09	0.95	9.24	71.90

CONCLUSIONS

A zinc-nicotinate complex, $\{[\text{Zn}(\text{na})_2(\mu\text{-pbix})]\cdot\text{H}_2\text{O}\}_n$ (**1**), was synthesized by using a mixed-ligand methodology under hydrothermal conditions. We used **Hna** and **pbix** as organic linkers and Zn salt as the metal source to construct a new CP, complex **1**. Complex **1** displays a 1D chain structure, and the chains are further linked by hydrogen bonds interactions to form high dimensional supramolecular structures. The IR spectrum confirms the coordination of carboxylate oxygen of the nicotinate with the metal ion, Zn. The fluorescence emissions show that complex **1** may be a good candidate for photoactive materials. We finally performed molecular simulations to compute single-component H₂ adsorption isotherms of complex **1** at 298 K and 77 K up to 1 bar. Results showed that complex **1** can be used as an adsorbent material to capture H₂ at 77 K.

ACKNOWLEDGEMENTS

The authors acknowledge to Scientific and Technological Research Application and Research Center, Sinop University, Turkey, for the use of the Bruker D8 QUEST diffractometer.

REFERENCES

1. Mai HD, Rafiq K, Yoo H. Nano Metal-Organic Framework-Derived Inorganic Hybrid Nanomaterials: Synthetic Strategies and Applications. *Chem-Eur J*. 2017;23(24):5631-51.
2. Janiak C. Engineering coordination polymers towards applications. *Dalton T*. 2003:2781-804.
3. Arici M, Yesilel OZ, Keskin S, Sahin O. Gas adsorption/separation properties of metal directed self-assembly of two coordination polymers with 5-nitroisophthalate. *J Solid State Chem*. 2014;210(1):280-6.
4. Semerci F, Yesilel OZ, Soylu MS, Keskin S, Buyukgungor O. A two-dimensional photoluminescent cadmium(II) coordination polymer containing a new coordination mode of pyridine-2,3-dicarboxylate: Synthesis, structure and molecular simulations for gas storage and separation applications. *Polyhedron*. 2013;50(1):314-20.
5. Guang-Xiang L. Synthesis, Crystal Structure and Magnetic Property of a Copper(II) Coordination Polymer Constructed from Nicotinic Acid. *Chinese J Inorg Chem*. 2013;29(9):1914-20.
6. Ay B, Yag G, Yildiz E, Rheingold AL. Hydrothermal synthesis and characterization of $\{[\text{Ni}-2(\text{na})_4(\mu\text{-H}_2\text{O})]\cdot 2\text{H}_2\text{O}\}_n$ (HNA = nicotinic acid) and its heterogeneous catalytic effect. *Polyhedron*. 2015;88:164-9.
7. Zhang XJ, Wang WJ, Hu ZJ, Wang GN, Uvdal KS. Coordination polymers for energy transfer: Preparations, properties, sensing applications, and perspectives. *Coordin Chem Rev*. 2015;284:206-35.
8. Batten SR, Chen BL, Vittal JJ. Coordination Polymers/MOFs: Structures, Properties and Applications. *Chempluschem*. 2016;81(8):669-70.
9. Lou BY, He FD. Coordination polymers as potential solid forms of drugs: three zinc(II) coordination polymers of theophylline with biocompatible organic acids. *New J Chem*. 2013;37(2):309-16.
10. Yan L, Liu W, Li CB, Wang YF, Ma L, Dong QQ. Hydrogen bonded supra-molecular framework in inorganic-organic hybrid compounds: Syntheses, structures, and photoluminescent properties. *J Mol Struct*. 2013;1035:240-6.
11. Chen GF, Cao CZ. Hydrothermal synthesis and structural characterization of a zigzag-chain polymer of $\{[\text{p-MeBzIPh}_3\text{P}][\text{ZnCl}_2(\text{NA})]\}_n$ (NA = nicotinic acid). *J Coord Chem*. 2008;61(2):262-9.
12. Nie FM, Wang SY. Synthesis and characterization of two nicotinate-containing cadmium complexes in a tripodal ligand system. *J Coord Chem*. 2011;64(23):4145-56.
13. Hojnik N, Kristl M, Golobic A, Jaglicic Z, Drofenik M. The synthesis, structure and physical properties of lanthanide(III) complexes with nicotinic acid. *Cent Eur J Chem*. 2014;12(2):220-6.
14. Liu DS, Sui Y, Chen WT, Feng PY. Two New Nonlinear Optical and Ferroelectric Zn(II) Compounds Based on Nicotinic Acid and Tetrazole Derivative Ligands. *Cryst Growth Des*. 2015;15(8):4020-5.
15. Song YS, Yan B, Chen ZX. Hydrothermal synthesis, crystal structure and luminescence of four novel metal-organic frameworks. *J Solid State Chem*. 2006;179(12):4037-46.

16. Liu ZX. Synthesis, Crystal Structure and Biological Activity of a Polymeric Silver(I) Complex Derived From Nicotinic Acid. *Synth React Inorg M.* 2016;46(6):809-13.
17. Vargova Z, Zelenak V, Cisarova I, Gyoryova K. Correlation of thermal and spectral properties of zinc(II) complexes of pyridinecarboxylic acids with their crystal structures. *Thermochim Acta.* 2004;423(1-2):149-57.
18. Di YY, Hong YP, Kong YX, Yang WW, Tan ZC. Synthesis, characterization, and thermochemistry of the solid state coordination compound $Zn(Nic)_2 \cdot H_2O(s)$ (Nic = nicotinic acid). *J Chem Thermodyn.* 2009;41(1):80-3.
19. do Nascimento ALCS, Caires FJ, Gomes DJC, Gigante AC, Ionashiro M. Thermal behaviour of nicotinic acid, sodium nicotinate and its compounds with some bivalent transition metal ions. *Thermochim Acta.* 2014;575:212-8.
20. Du M, Li CP, Liu CS, Fang SM. Design and construction of coordination polymers with mixed-ligand synthetic strategy. *Coordin Chem Rev.* 2013;257(7-8):1282-305.
21. Bu XZ, Chen JQ, Hu MZ. A New Luminescent Zn(II) Coordination Polymer Constructed From Nicotinic Acid and 3,5-Diamino-1,2,4-Triazole Ligands. *Synth React Inorg M.* 2016;46(1):123-6.
22. Qin JS, Yuan S, Wang Q, Alsalmeh A, Zhou HC. Mixed-linker strategy for the construction of multifunctional metal-organic frameworks. *J Mater Chem A.* 2017;5(9):4280-91.
23. An Z, Gao J, Zhu L. Isomeric luminescent Zn(II) coordination polymers based on pyridinecarboxylate and 5-methyl-1H-tetrazole ligands. *J Mol Struct.* 2013;1054:234-8.
24. Gao JY, Xiong XH, Chen CJ, Xie WP, Ran XR, Yue ST. Syntheses, Structures, and Fluorescence of Two Novel 2D Zinc(II) Layered Frameworks Based on 3-Amino-1, 2, 4-triazole. *Z Anorg Allg Chem.* 2013;639(3-4):582-6.
25. Liu DS, Huang XH, Huang CC, Huang GS, Chen JZ. Synthesis, crystal structures and properties of three new mixed-ligand d(10) metal complexes constructed from pyridinecarboxylate and in situ generated amino-tetrazole ligand. *J Solid State Chem.* 2009;182(7):1899-906.
26. Yuan G, Shao KZ, Chen L, Liu XX, Su ZM, Ma JF. Synthesis, crystal structures, and luminescent properties of Cd(II) coordination polymers assembled from semi-rigid multi-dentate N-containing ligand. *J Solid State Chem.* 2012;196:87-92.
27. Hu JM, Zhao YQ, Yu BY, Van Hecke K, Cui GH. Synthesis and Characterization of Two Distinct 2D Nickel(II) Coordination Polymers From Dicarboxylate and Flexible Bis(imidazole) Ligands. *Z Anorg Allg Chem.* 2016;642(1):41-7.
28. Erer H, Yesilel OZ, Arici M. A Series of Zinc(II) 3D \rightarrow 3D Interpenetrated Coordination Polymers Based On Thiophene-2,5-dicarboxylate and Bis(Imidazole) Derivative Linkers. *Cryst Growth Des.* 2015;15(7):3201-11.
29. Semerci F, Yesilel OZ, Yuksel F. Self-assembly of three new metal organic coordination networks based on 1,2-bis(imidazol-1yl-methyl)benzene. *Polyhedron.* 2015;102:1-7.
30. Arici M, Yesilel OZ, Tas M. Cd(II)-coordination polymers based on tetracarboxylic acid and diverse bis(imidazole) ligands: Synthesis, structural diversity and photoluminescence properties. *J Solid State Chem.* 2017;245:146-51.
31. Zou RQ, Abdel-Fattah AI, Xu HW, Zhao YS, Hickmott DD. Storage and separation applications of nanoporous metal-organic frameworks. *Crystengcomm.* 2010;12(5):1337-53.
32. So YH. Novel Thermoset Polyimidazole Amides. *Macromolecules.* 1992;25(2):516-20.
33. Tian ZF, Lin JG, Su Y, Wen LI, Liu YM, Zhu HZ, et al. Flexible ligand, structural, and topological diversity: Isomerism in $Zn(NO_3)_2$ coordination polymers. *Crystal Growth & Design.* 2007;7(9):1863-7.

34. Hoskins BF, Robson R, Slizys DA. An infinite 2D polyrotaxane network in $\text{Ag}_2(\text{bix})_3(\text{NO}_3)_2$ (bix=1,4-bis(imidazol-1-ylmethyl)benzene). *Journal of the American Chemical Society*. 1997;119(12):2952-3.
35. Dolomanov OV, Bourhis LJ, Gildea RJ, Howard JAK, Puschmann H. OLEX2: a complete structure solution, refinement and analysis program. *Journal of Applied Crystallography*. 2009;42(2):339-41.
36. Sheldrick GM. A short history of SHELX. *Acta Crystallographica Section A*. 2008;64(1):112-22.
37. Macrae CF, Edgington PR, McCabe P, Pidcock E, Shields GP, Taylor R, et al. Mercury: visualization and analysis of crystal structures. *J Appl Crystallogr*. 2006;39(3):453-7.
38. Allen FH. The Cambridge Structural Database: a quarter of a million crystal structures and rising. *Acta Crystallogr B*. 2002;58:380-8.
39. Willems TF, Rycroft C, Kazi M, Meza JC, Haranczyk M. Algorithms and tools for high-throughput geometry-based analysis of crystalline porous materials. *Micropor Mesopor Mat*. 2012;149(1):134-41.
40. Buch V. Path-Integral Simulations of Mixed Para-D2 and Ortho-D2 Clusters - the Orientational Effects. *Abstr Pap Am Chem S*. 1994;208:119-Phys.
41. Rappe AK, Casewit CJ, Colwell KS, Goddard WA, Skiff WM. Uff, a Full Periodic-Table Force-Field for Molecular Mechanics and Molecular-Dynamics Simulations. *J Am Chem Soc*. 1992;114(25):10024-35.
42. Erucar I, Keskin S. High CO₂ Selectivity of an Amine-Functionalized Metal Organic Framework in Adsorption-Based and Membrane-Based Gas Separations. *Ind Eng Chem Res*. 2013;52(9):3462-72.
43. Garberoglio G. Computer simulation of the adsorption of light gases in covalent organic frameworks. *Langmuir*. 2007;23(24):12154-8.
44. D. Frenkel, Smit B. *Understanding Molecular Simulation*. Elsevier Science 2001. 664 p.
45. Zelenak V, Vargova Z, Gyoryova K. Correlation of infrared spectra of zinc(II) carboxylates with their structures. *Spectrochim Acta A*. 2007;66(2):262-72.
46. Wu LJ, Li XX, Wang RH. Synthesis and Characterization of a Silver(I)-indium(III) Heterometallic Metal-organic Framework Based on Nicotinate. *Chinese J Struc Chem*. 2015;34(11):1703-8.
47. Meng XM, Zhang X, Qi PF, Zong ZA, Jin F, Fan YH. Syntheses, structures, luminescent and photocatalytic properties of various polymers based on a "V"-shaped dicarboxylic acid. *Rsc Adv*. 2017;7(9):4855-71.